

Electrical pumping of h -BN single-photon sources in van der Waals heterostructures

Mihyang Yu,[†] Jeonghan Lee,[†] Kenji Watanabe,[‡] Takashi Taniguchi,[‡] and Jieun Lee^{†}*

[†]Department of Physics and Astronomy, Seoul National University, Seoul, 08826, Korea

[‡]Research Center for Functional Materials, National Institute for Materials Science, Tsukuba,
305-0044, Japan

* To whom correspondence should be addressed, lee.jieun@snu.ac.kr.

Single-photon sources, hexagonal boron nitride, van der Waals heterostructures

Atomic defects in solids offer a versatile basis to study and realize quantum phenomena and information science in various integrated systems. All-electrical pumping of single defects to create quantum light emission has been realized in several platforms including color centers in diamond, silicon carbide, and zinc oxide, which could lead to the circuit network of electrically triggered single-photon sources. However, a wide conduction channel which reduces the carrier injection per defect site has been a major obstacle. Here, we conceive and realize a novel device concept to construct electrically pumped single-photon sources using a van der Waals stacked structure with atomic plane precision. Defect-induced tunneling currents across graphene and NbSe₂ electrodes sandwiching an atomically thin h -BN layer allows persistent and repeatable generation

of non-classical light from *h*-BN. The collected emission photon energies range between 1.4 and 2.9 eV, revealing the electrical excitation of a variety of atomic defects. By analyzing the dipole axis of observed emitters, we further confirm that emitters are crystallographic defect complexes of h-BN crystal. Our work facilitates implementing efficient and miniaturized single-photon devices in van der Waals platforms toward applications in quantum optoelectronics.

Defects in solid-state systems provide a rich platform to study not only the fundamental properties of materials and their modifications but also the quantum nature of the isolated carriers which find applications in quantum technologies.¹⁻⁵ Among various systems, two-dimensional materials provide an exceptional playground to study fundamental properties of defects regarding the dimensionality of the host material as well as their quantum nature for developing highly integrated quantum circuitries.⁶⁻⁸ For example, defects in ultrathin hexagonal boron nitride (*h*-BN) have been shown to exhibit bright single-photon emission that can be used for quantum communication^{9,10} and single spins that can probe minute physical quantities of proximate specimens in nanometer distance.¹¹⁻¹³ However, implementing quantum operation of *h*-BN defects in previous works have largely relied on the optical pumping source for the generation of carriers which imposes difficulties on the targeted and controlled manipulations of defects in integrated structures.

Electrical excitation of single defects, on the other hand, offers an appealing opportunity to selectively control quantum emitters in designated locations in electrical devices without the inclusion of the laser source that excites background signals.^{14,15} Two-dimensional van der Waals materials provide a particularly suitable material platform for such device structure through the nanometer scale tailoring of the host material and electrodes. In this structure, the direct carrier injection into the local defects using a voltage also leverages the

charge control of defects which will be potentially useful for synchronized and ultrafast manipulation of multiple quantum emitters with increased scalability. However, the electrical excitation of an isolated defect and single-photon generation in *h*-BN has not been demonstrated so far.

In this article, we report the direct electrical pumping of single-photon emitters in *h*-BN embedded in electronic devices with atomically thin thicknesses. By fabricating van der Waals heterostructures composed of *h*-BN, graphene, and NbSe₂, we established the electrical generation of single-photon emission by direct carrier injection. The electrically induced photon emission shows the intensity that scales linearly with the applied current and exhibits antibunching in the photon correlation measurement using a Hanbury, Brown, and Twiss interferometer. The asymmetric layer configuration of the van der Waals heterostructure formation also enables the stable generation of single-photon emission, allowing the analysis of characteristic photon energies and polarization axes of the emitters. Our work on the electrically pumped generation of *h*-BN single-photon emission will open possible applications of *h*-BN defects for miniaturized compact single-photon devices and chip-based quantum information science.

Results and Discussion

The device structure is illustrated in Fig. 1a. A few-layer NbSe₂ and graphene were used as top and bottom metallic electrode, respectively, for applying tunneling current through optically active *h*-BN defect sites. For creating optically active defects in *h*-BN, high temperature annealing with O₂ gas flow was performed on a *h*-BN layer with thickness of 5 nm.¹⁶ A thin *h*-BN spacer layer (2 nm) is inserted between the optically active *h*-BN and top NbSe₂ as part of a sequential transfer of multilayer stacking. See SI section 1 for more details.

By applying a voltage across two electrodes, the charge current flow through the defect was generated which induces the electrical pumping of the emitter luminescence.

In the heterostructure, the combination of NbSe₂, a hole-like van der Waals metal,^{17,18} and graphene is chosen to form an asymmetric electrical junction with *h*-BN in between, enabling the efficient injection of electron and hole carriers into the defect sites for the generation of single-photon emission. In addition, the edge of two metallic electrodes were aligned with minimal overlap, confining the path of the tunneling current flow to go through the defects positioned within the aligned edges. Reducing the number of defects participating in the tunneling current generation further stabilizes the photon emission and allows the direct comparison of the emission intensity with respect to the tunneling current.

With the fabricated device, we measured the electroluminescence (EL) from *h*-BN defect sites in an optical set-up equipped with a cryostat kept at 6.5 K while varying the applied voltage. Fig. 1b shows the electrically induced emission spectrum measured from a localized position of a device showing several narrow emission peaks brightened as a function of voltage. Above a threshold, the emission intensity of individual peaks gradually increases as voltage increases. The spatial image measured by the charge-coupled device (CCD) imaging mode is shown in Fig. 1c. From the image depicting the reflection of a white light source, the boundaries of two electrodes can be identified and the localized EL ($V = 28$ V) is found at one corner of the stacked region.

Fig. 1d shows the line spectra of the emitters measured at the applied voltage of 0 and 30 V. The emission peaks at 1.5, 2.8, and 2.9 eV are identified as the zero-phonon lines (ZPLs) of single defects. The small peak at 2.6 eV is the phonon sideband of the ZPL peak at 2.8 eV, as confirmed from the energy separation (160 meV) matching with the longitudinal optical phonons of *h*-BN¹⁹ and the simultaneous spectral shift of the two peaks found from the time

stability measurement (SI section 2). Other emitter peaks around 1.5 and 2.9 eV exhibited low energy phonon sidebands which are close to the ZPL emission lines. Such variation of phonon sidebands originates from the layered structure of the host material²⁰ and agrees with the previous reports of *h*-BN quantum emitters.^{21,22}

We then performed more detailed measurements of the emitter with ZPL energy at 1.5 eV, which are presented in Fig. 2. The high-resolution spectra of this emitter with varying voltage are shown in Fig. 2a and b, indicating that the peak starts to emerge at the threshold voltage of about 26 V. A noticeable Stark shift is also found as a function of voltage, representing the existence of the out-of-plane dipole moment of the emitter.^{23–25} By plotting the sum of the emitter’s peak intensity and tunneling current together as a function of voltage (Fig. 2c), the emission intensity is found to scale linearly with the tunneling current, starting with the same threshold voltage. This unambiguously shows that tunneling current is induced by defect-mediated charge transport which directly contributes to the charge carrier supply at the emitter site. In SI section 3, we present the real-time measurement of the correlation between photon intensity and tunneling current measured from another device which further supports the defect-induced current flow, a distinct behavior enabled by the van der Waals device scheme.

Next, the single-photon emission property of the emitter is manifested by carrying out the second order correlation function measurement. Fig. 2d shows the correlation function recorded for the emitter under the applied current magnitude of about 6 nA. After the background correction,²⁶ we obtained the $g^2(0)$ value of 0.25 ± 0.21 , proving the quantum nature of the electrically pumped defect emission in *h*-BN. The width of the dip extracted from the fitting function is 18.2 ± 7.2 ns, larger than typical lifetimes measured from optically excited emitters (\sim a few ns),^{7,27,28} implying that additional charge-trapping levels could have been

involved in the transition process.¹⁴ We also note that this is the first demonstration of the quantum light emission from *h*-BN via electrical pumping, which will be advantageous for future applications of point defects in van der Waals devices for quantum technologies.^{29,30}

Fig. 2e shows the linear polarization of this emitter verified by a polarization-resolved experiment. While applying a voltage, the polarization of the emitted light is selected by an analyzer in front of the CCD detector with angle θ measured relative to the high symmetry axis of the *h*-BN crystal. By fitting the polar plot of the angle-resolved intensity by using $I(\theta) = A\cos^2(\theta + \theta_0) + B$, we find θ_0 of about 60° for this emitter. We investigate the polarization measurement results of all emitters measured from the same device more closely in relation to the wavelength distribution below.

The observed emitter also showed remarkable stability in terms of the emission intensity and wavelength as can be seen in Fig. 2f. The emission intensity exhibits generally persistent values with a few intermittent brightening, which could have originated from nearby charging impurities.³¹ The emitter also showed consistent emission properties that could be reproduced after turning the voltage off and on again over several tens of hours, supporting the robustness of the electrical pumping source for generating photon emission (SI section 4).

Furthermore, by applying a high voltage to the device above 60 V, we could observe that more emitters are created in the device in addition to the pre-existing emitters (SI section 5). After applying a high voltage, several sharp peaks emerged which have similar energy and polarization characteristics with previously reported *h*-BN defects.^{21,32-35} The creation of new defect levels can have several possible causes. The charge state of existing defects can be changed due to carrier injection through a high voltage³⁶ or new defect sites can be created by the breaking of B-N bonding in *h*-BN and coupling with adjacent layers³⁷⁻³⁹ or ions.⁴⁰⁻⁴² In our experiment, more than 50 emitters are observed including the pre-existing and newly created

defects which showed stable emission properties.

To understand the electrically pumped emission mechanism, we collected histograms of the emission wavelength of the observed emitters arising at positive and negative voltages which are shown in Fig. 3a and b, respectively. The result reveals two evident characteristics. First, the number of emitters appearing at positive voltages far exceeds that appearing at negative voltages. Second, at higher photon energies, most emitters are observed under the application of positive voltages with only a few exceptions.

Our observation is fully compatible with the band diagram of the device structure shown in Fig. 3c. Because of the different work function of graphene ($W_G = 4.5$ eV)^{43,44} and NbSe₂ ($W_{NbSe_2} = 5.9$ eV),⁴⁵ the heterostructure at zero bias creates a built-in band tilting in *h*-BN and the Fermi level of NbSe₂ is close to the *h*-BN valence band maximum. By applying a finite voltage, current flow supplies electrons and holes into the defect sites, leading to photon emission through the carrier transition. This process occurs more efficiently under a positive bias because NbSe₂, a hole metal, preferentially provides hole carriers for the tunneling current. The supply of holes from NbSe₂ and electrons from graphene allows the stable generation of photons at the defect location. At a negative voltage, electron carriers are less supplied, resulting in a lower probability of photon emission, which is more pronounced for emitters with higher transition energies.

We now investigate the possible crystallographic origins of the emitters in our experiment. From the measurement, we categorize the emitters into three different groups based on their wavelengths: the short-wavelength group (Group 1) with the energy 2.4 – 3.0 eV, the middle-wavelength group (Group 2) with the energy 1.9 – 2.4 eV, and the long-wavelength group (Group 3) with the energy 1.4 – 1.7 eV. The categorization is also indicated by the dashed lines in Fig. 3a. Different groups show characteristic photon energy, the shape

of phonon sidebands, and polarization dependence as shown in Fig. 4, implying that they have different origins.

Group 1 emitters showed phonon sidebands that are about 170 meV apart from the ZPL and axes of the linear polarization which are generally separated by a 60-degree interval. Such polarization dependence agrees with the recently observed emitters that are induced by e-beam irradiation^{32,33} or carbon ion implantation.³⁴ The observation suggests that group 1 emitters have a high possibility to originate from carbon-related color centers. Conversely, group 3 emitters showed negligibly small phonon sidebands and randomized distribution of polarization axes. The emission energy range and the shape of the spectrum matches well with that of oxygen-related defect centers.^{35,46} We emphasize that the abundance of group 3 emitters from the experiment could be the result of the oxygen flow annealing process during the fabrication. From other devices fabricated using argon-annealed *h*-BN layers, strikingly contrasting emitter distribution is found (SI section 6). Our work thus highlights the accessibility of EL experimental tool to probe oxygen-related single photon sources in *h*-BN crystal. Group 2 emitters, in between, showed a wide range of variation in both the spectral shape and polarization distribution. Further research on electrically driven defect emission created by more controlled fabrication methods will unveil additional information on the defect identification, charge control, and emission mechanism of *h*-BN single-photon sources.

Conclusions

In conclusion, we demonstrated all-electrical generation of single-photon emission from *h*-BN by incorporating van der Waals integrated device scheme. The combination of graphene and NbSe₂ as electrode materials in an asymmetric device structure enables the stable generation of photon emission in a wide range of spectral windows, allowing studies on various types of quantum emitters with electrical excitation. We anticipate expanding the horizon of

two-dimensional materials in heterostructure fabrication design involving *h*-BN defects will promote the functionality and applicability of quantum technologies using van der Waals quantum optoelectronics. Through integrable single-photon sources in ultrathin materials with electrical excitation capabilities, further progress in electrically driven quantum communication⁴⁷ and spin defect operations⁴⁸ will be possible.

Methods

All optical measurements are performed with a home-built confocal microscopy set-up. The luminescence signal from the sample is collected using an objective lens with the numerical aperture of 0.65, passed through the collection path, and entered either a spectrometer or a Hanbury, Brown, and Twiss interferometer set-up.

For the characterization of the emitters, the spatial image of the emission is collected by setting the grating of the spectrometer in the zeroth-order position, which functions as a mirror to detect the 2D map of the electrically activated emitters at the CCD position. Outline of the sample boundaries are obtained by using a white-light source. To detect the voltage-dependent emitter spectra, photons emitted from the defect centers are dispersed by a diffraction grating in the spectrometer and recorded by the CCD in the spectrum mode. The polarization dependence of the emitted signal is obtained by using a polarizer and a half-wave plate in the rotating mount in the collection path.

In the Hanbury, Brown, and Twiss interferometer set-up, the emission signal is split by 50:50 beam splitter in the collection path and recorded by two avalanche photodiodes (APDs). The APDs are connected to a time-correlated single-photon counting device for monitoring the second-order correlation function and temporal stability of the emitter luminescence.

Acknowledgement

We acknowledge support from the National Research Foundation of Korea (NRF) grant funded by the Korea government (MSIT) (No. 2020R1A2C201133414, No. 2021R1A5A103299614, and No. RS-2024-00356893) and the Institute for Basic Science (IBS) in Korea (No. IBS-R009_D1). The research is further supported by the ITRC (Information Technology Research Center) support program (RS-2022-00164799) supervised by the IITP (Institute for Information & communications Technology Promotion) of Korea.

References

- (1) Wolfowicz, G.; Heremans, F. J.; Anderson, C. P.; Kanai, S.; Seo, H.; Gali, A.; Galli, G.; Awschalom, D. D. Quantum guidelines for solid-state spin defects. *Nat. Rev. Mater.* **2021**, *6* (10), 906–925.
- (2) Aharonovich, I.; Englund, D.; Toth, M. Solid-state single-photon emitters. *Nat. Photonics* **2016**, *10* (10), 631–641.
- (3) Schröder, T.; Mouradian, S. L.; Zheng, J.; Trusheim, M. E.; Walsh, M.; Chen, E. H.; Li, L.; Bayn, I.; Englund, D. Quantum nanophotonics in diamond [Invited]. *J. Opt. Soc. Am. B* **2016**, *33* (4), B65–B83.
- (4) Lohrmann, A.; Johnson, B. C.; McCallum, J. C.; Castelletto, S. A review on single photon sources in silicon carbide. *Rep. Prog. Phys.* **2017**, *80* (3), 034502.
- (5) Morfa, A. J.; Gibson, B. C.; Karg, M.; Karle, T. J.; Greentree, A. D.; Mulvaney, P.; Tomljenovic-Hanic, S. Single-photon emission and quantum characterization of zinc oxide defects. *Nano Lett.* **2012**, *12* (2), 949–954.
- (6) Chakraborty, C.; Vamivakas, N.; Englund, D. Advances in quantum light emission from 2D materials. *Nanophotonics* **2019**, *8* (11), 2017–2032.
- (7) Shaik, A. B. Dhu-al-jalali-wal-ikram; Palla, P. Optical quantum technologies with hexagonal boron nitride single photon sources. *Sci. Rep.* **2021**, *11* (1), 12285.
- (8) Tran, T. T.; Bray, K.; Ford, M. J.; Toth, M.; Aharonovich, I. Quantum emission from hexagonal boron nitride monolayers. *Nat. Nanotech.* **2016**, *11* (1), 37–41.
- (9) Samaner, Ç.; Paçal, S.; Mutlu, G.; Uyanık, K.; Ateş, S. Free-space quantum key distribution with single photons from defects in hexagonal boron nitride. *Adv. Quantum Technol.* **2022**, *5* (9), 2200059.

- (10) Al-Juboori, A.; Zeng, H. Z. J.; Nguyen, M. A. P.; Ai, X.; Laucht, A.; Solntsev, A.; Toth, M.; Malaney, R.; Aharonovich, I. Quantum key distribution using a quantum emitter in hexagonal boron nitride. *Adv. Quantum Technol.* **2023**, *6* (9), 2300038.
- (11) Vaidya, S.; Gao, X.; Dikshit, S.; Aharonovich, I.; Li, T. Quantum sensing and imaging with spin defects in hexagonal boron nitride. *Adv. Phys. X* **2023**, *8* (1), 2206049.
- (12) Gottscholl, A.; Diez, M.; Soltamov, V.; Kasper, C.; Krauße, D.; Sperlich, A.; Kianinia, M.; Bradac, C.; Aharonovich, I.; Dyakonov, V. Spin defects in hBN as promising temperature, pressure and magnetic field quantum sensors. *Nat. Commun.* **2021**, *12* (1), 4480.
- (13) Healey, A. J.; Scholten, S. C.; Yang, T.; Scott, J. A.; Abrahams, G. J.; Robertson, I. O.; Hou, X. F.; Guo, Y. F.; Rahman, S.; Lu, Y.; et al. Quantum microscopy with van der Waals heterostructures. *Nat. Phys.* **2023**, *19* (1), 87–91.
- (14) Mizuochi, N.; Makino, T.; Kato, H.; Takeuchi, D.; Ogura, M.; Okushi, H.; Nothaft, M.; Neumann, P.; Gali, A.; Jelezko, F.; et al. Electrically driven single-photon source at room temperature in diamond. *Nat. Photonics* **2012**, *6* (5), 299–303.
- (15) Lohrmann, A.; Iwamoto, N.; Bodrog, Z.; Castelletto, S.; Ohshima, T.; Karle, T. J.; Gali, A.; Prawer, S.; McCallum, J. C.; Johnson, B. C. Single-photon emitting diode in silicon carbide. *Nat. Commun.* **2015**, *6* (1), 7783.
- (16) Chen, Y.; Li, C.; White, S.; Nonahal, M.; Xu, Z. Q.; Watanabe, K.; Taniguchi, T.; Toth, M.; Tran, T. T.; Aharonovich, I. Generation of high-density quantum emitters in high-quality, exfoliated hexagonal boron nitride. *ACS Appl. Mater. Interfaces* **2021**, *13* (39), 47283–47292.
- (17) Mattheiss, L. F. Band structures of transition-metal-dichalcogenide layer compounds. *Phys. Rev. B* **1973**, *8* (8), 3719–3740.
- (18) Johannes, M. D.; Mazin, I. I.; Howells, C. A. Fermi-surface nesting and the origin of the charge-density wave in NbSe₂. *Phys. Rev. B* **2006**, *73* (20), 205102.
- (19) Serrano, J.; Bosak, A.; Arenal, R.; Krisch, M.; Watanabe, K.; Taniguchi, T.; Kanda, H.; Rubio, A.; Wirtz, L. Vibrational properties of hexagonal boron nitride: Inelastic X-ray scattering and *ab initio* calculations. *Phys. Rev. Lett.* **2007**, *98* (9), 095503.
- (20) Khatri, P.; Luxmoore, I. J.; Ramsay, A. J. Phonon sidebands of color centers in hexagonal boron nitride. *Phys. Rev. B* **2019**, *100* (12), 125305.
- (21) Exarhos, A. L.; Hopper, D. A.; Grote, R. R.; Alkauskas, A.; Bassett, L. C. Optical signatures of quantum emitters in suspended hexagonal boron nitride. *ACS Nano* **2017**, *11* (3), 3328–3336.
- (22) Jungwirth, N. R.; Fuchs, G. D. Optical absorption and emission mechanisms of single defects in hexagonal boron nitride. *Phys. Rev. Lett.* **2017**, *119* (5), 057401.
- (23) Noh, G.; Choi, D.; Kim, J. H.; Im, D. G.; Kim, Y. H.; Seo, H.; Lee, J. Stark tuning of single-photon emitters in hexagonal boron nitride. *Nano Lett.* **2018**, *18* (8), 4710–4715.
- (24) Xia, Y.; Li, Q.; Kim, J.; Bao, W.; Gong, C.; Yang, S.; Wang, Y.; Zhang, X. Room-temperature giant Stark effect of single photon emitter in van der Waals material. *Nano Lett.* **2019**, *19* (10), 7100–7105.

- (25) Nikolay, N.; Mendelson, N.; Sadzak, N.; Böhm, F.; Tran, T. T.; Sontheimer, B.; Aharonovich, I.; Benson, O. Very large and reversible Stark-shift tuning of single emitters in layered hexagonal boron nitride. *Phys. Rev. Appl.* **2019**, *11* (4), 041001.
- (26) Beveratos, A.; Kühn, S.; Brouri, R.; Gacoin, T.; Poizat, J. P.; Grangier, P. Room temperature stable single-photon source. *Eur. Phys. J. D* **2002**, *18* (2), 191–196.
- (27) Castelletto, S.; Inam, F. A.; Sato, S. I.; Boretti, A. Hexagonal boron nitride: A review of the emerging material platform for single-photon sources and the spin-photon interface. *Beilstein J. Nanotechnol.* **2020**, *11*, 740–769.
- (28) Akbari, H.; Biswas, S.; Jha, P. K.; Wong, J.; Vest, B.; Atwater, H. A. Lifetime-limited and tunable quantum light emission in *h*-BN via electric field modulation. *Nano Lett.* **2022**, *22* (19), 7798–7803.
- (29) Liu, X.; Hersam, M. C. 2D materials for quantum information science. *Nat. Rev. Mater.* **2019**, *4* (10), 669–684.
- (30) Turunen, M.; Brotons-Gisbert, M.; Dai, Y.; Wang, Y.; Scerri, E.; Bonato, C.; Jöns, K. D.; Sun, Z.; Gerardot, B. D. Quantum photonics with layered 2D materials. *Nat. Rev. Phys.* **2022**, *4* (4), 219–236.
- (31) Bishop, S. G.; Hadden, J. P.; Alzahrani, F. D.; Hekmati, R.; Huffaker, D. L.; Langbein, W. W.; Bennett, A. J. Room-temperature quantum emitter in aluminum nitride. *ACS Photonics* **2020**, *7* (7), 1636–1641.
- (32) Horder, J.; White, S. J. U.; Gale, A.; Li, C.; Watanabe, K.; Taniguchi, T.; Kianinia, M.; Aharonovich, I.; Toth, M. Coherence properties of electron-beam-activated emitters in hexagonal boron nitride under resonant excitation. *Phys. Rev. Appl.* **2022**, *18* (6), 064021.
- (33) Kumar, A.; Samaner, Ç.; Cholsuk, C.; Matthes, T.; Paçal, S.; Oyun, Y.; Zand, A.; Chapman, R. J.; Saerens, G.; Grange, R.; et al. Polarization dynamics of solid-state quantum emitters. *ACS Nano* **2023**, *18* (7), 5270–5281.
- (34) Zhong, D.; Gao, S.; Saccone, M.; Greer, J. R.; Bernardi, M.; Nadj-Perge, S.; Faraon, A. Carbon-related quantum emitter in hexagonal boron nitride with homogeneous energy and 3-fold polarization. *Nano Lett.* **2024**, *24* (4), 1106–1113.
- (35) Mohajerani, S. S.; Chen, S.; Alaei, A.; Chou, T.; Liu, N.; Ma, Y.; Xiao, L.; Lee, S. S.; Yang, E. H.; Strauf, S. Narrowband quantum light emission from oxygen-related color centers in hexagonal boron nitride. *ACS Photonics* **2024**, *11* (6), 2359–2367.
- (36) Yu, M.; Yim, D.; Seo, H.; Lee, J. Electrical charge control of *h*-BN single photon sources. *2D Mater.* **2022**, *9* (3), 035020.
- (37) Ranjan, A.; O’Shea, S. J.; Padovani, A.; Su, T.; La Torraca, P.; Ang, Y. S.; Munde, M. S.; Zhang, C.; Zhang, X.; Bosman, M.; et al. Molecular bridges link monolayers of hexagonal boron nitride during dielectric breakdown. *ACS Appl. Electron. Mater.* **2023**, *5* (2), 1262–1276.
- (38) Ganyecz, Á.; Babar, R.; Benedek, Z.; Aharonovich, I.; Barcza, G.; Ivády, V. First-principles theory of the nitrogen interstitial in hBN: a plausible model for the blue emitter. *Nanoscale* **2024**, *16* (8), 4125–4139.

- (39) Kumar, S.; Mishra, V.; Ganapathi, K. L.; Miryala, M.; Rao, M. S. R.; Dixit, T. Ab-initio investigations into Frenkel defects in hexagonal boron nitride for quantum optoelectronic applications. *IEEE Trans. Nanotechnol.* **2024**, *23*, 109–113.
- (40) Mendelson, N. *et al.* Identifying carbon as the source of visible single-photon emission from hexagonal boron nitride. *Nat. Mater.* **2021**, *20*, 321–328.
- (41) Maciaszek, M.; Razinkovas, L.; Alkauskas, A. Thermodynamics of carbon point defects in hexagonal boron nitride. *Phys. Rev. Mater.* **2022**, *6* (1), 014005.
- (42) Li, S.; Gali, A. Identification of an oxygen defect in hexagonal boron nitride. *J. Phys. Chem. Lett.* **2022**, *13* (41), 9544–9551.
- (43) Yu, Y. J.; Zhao, Y.; Ryu, S.; Brus, L. E.; Kim, K. S.; Kim, P. Tuning the graphene work function by electric field effect. *Nano Lett.* **2009**, *9* (10), 3430–3434.
- (44) Yan, R.; Zhang, Q.; Li, W.; Calizo, I.; Shen, T.; Richter, C. A.; Hight-Walker, A. R.; Liang, X.; Seabaugh, A.; Jena, D.; *et al.* Determination of graphene work function and graphene-insulator- semiconductor band alignment by internal photoemission spectroscopy. *Appl. Phys. Lett.* **2012**, *101* (2), 022105.
- (45) Shimada, T.; Ohuchi, F. S. Work function and photothreshold of layered metal dichalcogenides. *Jpn. J. Appl. Phys.* **1994**, *33* (5R), 2696.
- (46) Xu, Z. Q.; Elbadawi, C.; Tran, T. T.; Kianinia, M.; Li, X.; Liu, D.; Hoffman, T. B.; Nguyen, M.; Kim, S.; Edgar, J. H.; *et al.* Single photon emission from plasma treated 2D hexagonal boron nitride. *Nanoscale* **2018**, *10* (17), 7957–7965.
- (47) Couteau, C.; Barz, S.; Durt, T.; Gerrits, T.; Huwer, J.; Prevedel, R.; Rarity, J.; Shields, A.; Weihs, G. Applications of single photons to quantum communication and computing. *Nat. Rev. Phys.* **2023**, *5* (6), 326–338.
- (48) Siyushev, P.; Nesladek, M.; Bourgeois, E.; Gulka, M.; Hruby, J.; Yamamoto, T.; Trupke, M.; Teraji, T.; Isoya, J.; Jelezko, F. Photoelectrical imaging and coherent spin-state readout of single nitrogen-vacancy centers in diamond. *Science* **2019**, *363* (6428), 728–731.

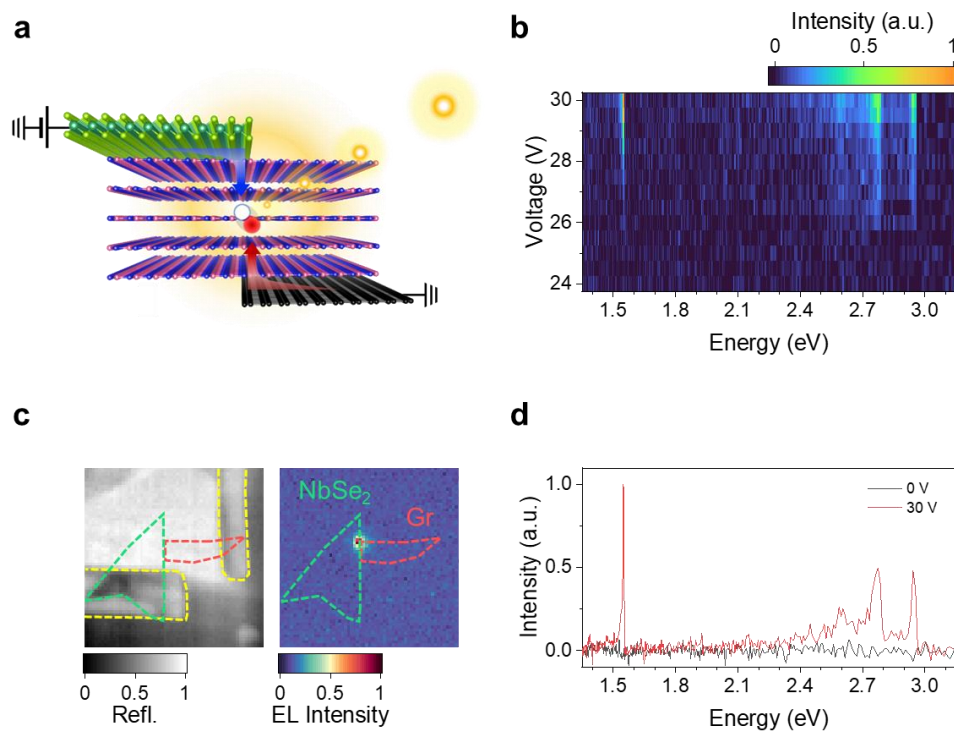


Figure 1. Electrically pumped defect emission from *h*-BN heterostructure device. (a) Schematics of *h*-BN heterostructure device with NbSe₂ and graphene electrodes. Red and white circles represent electron and hole carriers at the defect site. A stream of yellow open circles indicates the single-photon generation. **(b)** Color map of the voltage-dependent spectra. All data are normalized by the maximum intensity. **(c)** 2D spatial image obtained by CCD from white light reflection of the device (left) and electroluminescence emission at 28 V (right). Green, red, and yellow lines are NbSe₂, graphene, and Au electrodes, respectively. **(d)** Emission spectra measured at 0 (black) and 30 V (red).

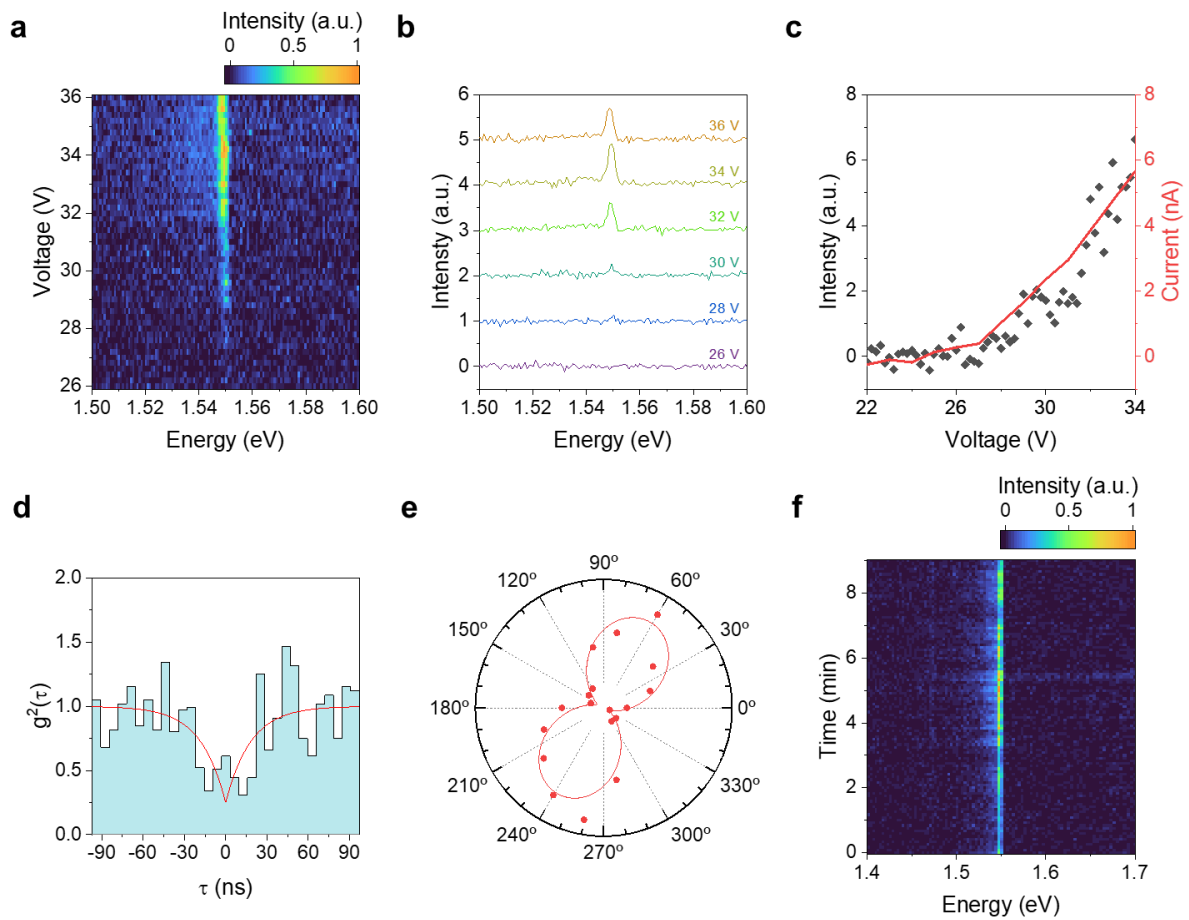


Figure 2. Voltage, polarization, and time dependence of a single-photon source. (a) High resolution color map of the voltage-dependent spectra of 1.5 eV emitter. **(b)** Spectra of the emitter at selected voltages. **(c)** Integrated emitter intensity (black dots) and simultaneously measured channel current (red line). **(d)** Second order correlation function $g^2(\tau)$ measurement (filled area) and fit function (red line). **(e)** Polar plot of the integrated intensity (black dots) and the fit result using $\cos^2(\theta)$ function (red line). **(f)** Time stability of the emitter measured at 30 V.

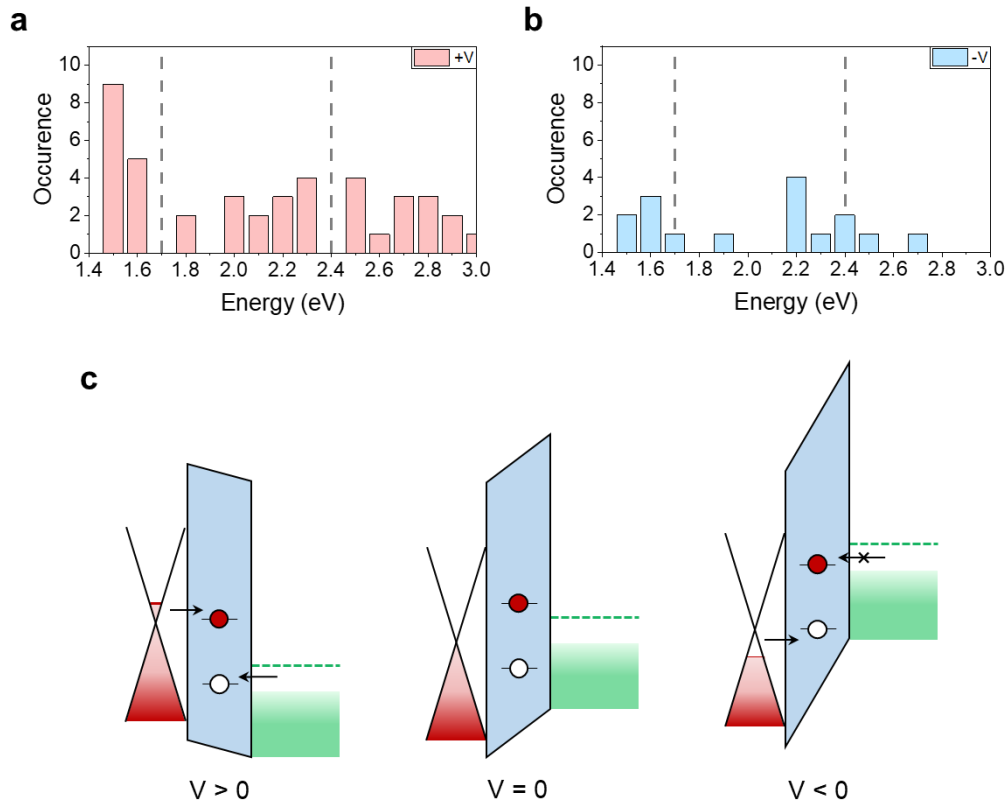


Figure 3. Emitter's energy distribution and charge injection mechanism. (a) Energy distribution of defect emitters activated under the application of positive voltages. Vertical dashed lines are shown to categorize the emitters into three different groups depending on the emission energy. **(b)** Energy distribution of defect emitters activated under the application of negative voltages. **(c)** Band diagram of graphene, *h*-BN, and NbSe₂ stacked heterostructure with positive (left), zero (middle), and negative (right) applied voltages. Red solid lines are the Fermi level of graphene and green dashed lines are the energy maximum of the partly filled hole band of NbSe₂. The built-in band tilting at zero voltage reflects the work function difference between graphene and NbSe₂.

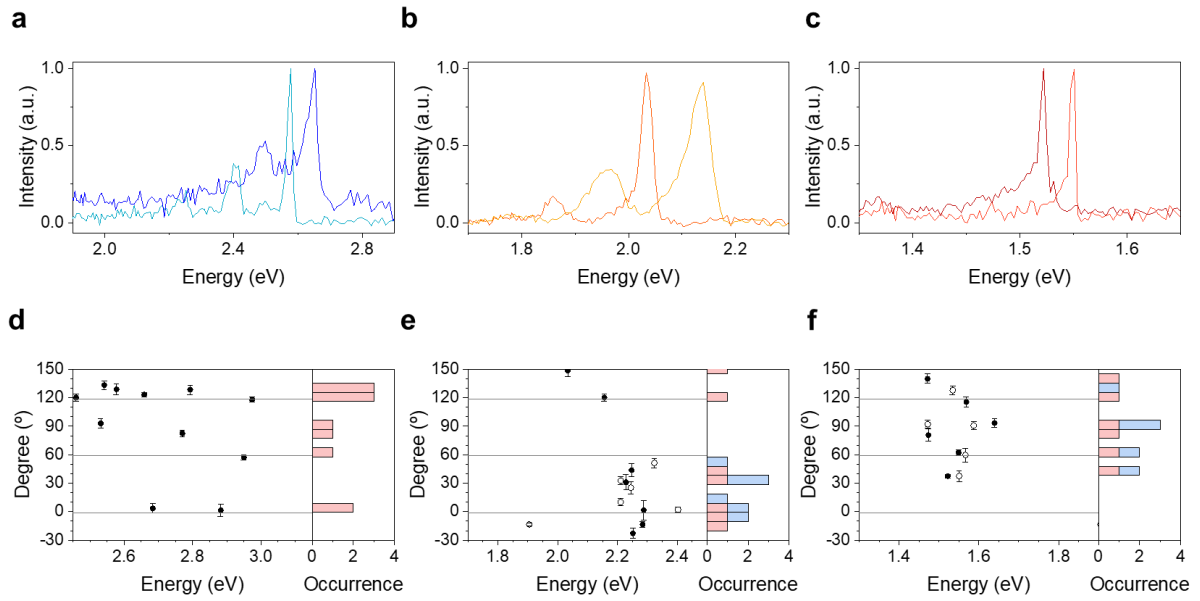


Figure 4. Polarization distribution of *h*-BN defects. (a,d) Short-wavelength group 1 emitters with representative spectra (a) and dipole moment axes found from polarization dependence measurement data (d). Filled and open circles indicate emitters with positive and negative threshold voltages, respectively. Occurrence as a function of polarization angle is shown together for emitters with positive (pink) and negative (blue) threshold voltages. **(b,e)** Middle-wavelength group 2 emitters with representative spectra (b) and dipole moment axes (e). **(c,f)** Long-wavelength group 3 emitters with representative spectra (c) and dipole moment axes (f).